A New Framework for Force Feedback Teleoperation of Robotic Vehicles based on Optical Flow

Robert Mahony, Felix Schill, Peter Corke and Yoong Siang Oh

***Abstract*— This paper proposes the use of optical flow from a moving robot to provide force feedback to an operator's joystick to facilitate collision free teleoperation. Optic flow is measured by wide angle cameras on board the vehicle and used to generate a *virtual* environmental force that is reflected to the user through the joystick, as well as feeding back into the control of the vehicle. The coupling between optical flow (velocity) and force is modelled as an impedance – in this case an *optical* impedance. We show that the proposed control is dissipative and prevents the vehicle colliding with the environment as well as providing the operator with a natural feel for the remote environment.**

The paper focuses on applications to aerial robotics vehicles, however, the ideas apply directly to other force actuated vehicles such as submersibles or space vehicles, and the authors believe the approach has potential for control of terrestrial vehicles and even teleoperation of manipulators. Experimental results are provided for a simulated aerial robot in a virtual environment controlled by a haptic joystick.

I. INTRODUCTION

Unmanned aerial and submersible vehicles have an important role to play as remote surveillance platforms to remove human operators from dangerous and difficult situations. Commercial applications exist in inspection of infrastructure such as piping, cabling, etc, for a range of industrial and civil settings as well as the more publicised search and rescue and crowd surveillance scenarios.

A key requirement of a vehicle functioning in such a role is a capability to manoeuvre safely in cluttered three-dimensional scenarios such as indoor or urban canyon environments. Existing systems require the undivided attention of highly skilled operators and normally require line of sight to the actual vehicle. The application of teleoperated mini aerial robots to these applications is gaining interest [9] with the goal of developing systems that can be controlled intuitively by someone with only minimal training.

Safe teleoperation of robotic vehicles in cluttered environments requires an integrated obstacle avoidance capability based on exteroceptive sensor systems. One of the most promising sensor modalities for obstacle avoidance in robotics is the use of vision, and particularly optic flow [4], [13], [16], [17]. Motivation for this approach in aerial robots is drawn from the study of vision and flight in insects [24]. Recently there has been considerable interest in using optic flow velocity cues for control of aerial vehicles [2], [8], [18], [20], [21], [26]. The authors know of no prior reference for use of optic flow in teleoperation of robotic vehicles.

In this paper, we provide an integrated framework for teleoperation of robotic vehicles that provides the operator with a haptic feel for obstacles in the environment based on optic flow measured by the vehicle. We treat optic flow, or a derivative of optic flow such as optical divergence, as a velocity variable induced by the motion of the robot in the environment, and then implement a force that proportionally opposes this motion both directly on the vehicle, and also as a reflected force experienced by the operator through a haptic user interface.

The key idea of the approach is the definition of *optical impedance*, a mapping from the optical flow field to forces on the vehicle. Modelling the system in this manner leads to an energy flow model of the closed-loop vehicle dynamics. We propose two optical impedances: Firstly spherical divergence computed at the focus of expansion, a dissipative impedance that acts to prevent collision with the environment, and secondly a differential flow impedance, a passive impedance that acts to centre the vehicle in corridor like environments without opposing forward motion.

The paper is written in the context of aerial robotic vehicles but the technique is directly applicable to other thrust controlled vehicles such as submersibles and space vehicles. However, we believe that the underlying concept optical impedance has broader application and is relevant to teleoperation of all robotic vehicles and even of robotic manipulators, although space limitations in this paper prevent us from going into details. In particular, we mention recent work [22] where some initial experimental results are presented on a holonomic robotic vehicle. In this paper, the performance of the proposed control strategy is demonstrated in a 3-D simulation environment. The experiments carried out in the simulation are a precursor to an implementation on a quadrotor aerial robot with panoramic vision sensors

After this introduction, Section II introduces the dynamic system models. Section III defines the concept of optical impedance and uses a simple example to provide insight into the proposed approach. Section IV introduces the two optical impedances that we propose as 'good' choices. Section V discusses the experiment setup developed and presents some results.

II. P

In this section we develop dynamic models of an aerial robotic vehicle and the 3D-haptic user interface independently and as an integrated system.

R. Mahony, F. Schill and Y. Oh are with Department of Engineering, Australian National University, ACT, 0200, AUSTRALIA, {firstname}.{lastname}@anu.edu.au

P. Corke is with CSIRO ICT Centre, Pullenvale, Queensland, AUSTRALIA. peter.corke@csiro.au

A. Dynamic Model for a hovering UAV

We consider the case of an aerial robotic vehicle capable of quasi-stationary flight, that is hover and near-hover flight. The system model considered is based on those introduced in the literature to model the dynamics of helicopters [6], [23] and helicopter like vehicles [11], [19].

Let $\{A\}$ denote the inertial reference frame, fixed to the earth surface, and let $\{B\}$ denote the airframe, a body-fixed frame attached to the vehicle. The position of the airframe in the world frame is denoted $x \in \{A\}$ and its attitude (or orientation) is given by a rotation matrix R representing the attitude of frame $\{B\}$ with respect to $\{A\}$. Let $v \in \{A\}$ denote the translational velocity and $\Omega \in \{B\}$ denote the angular velocity. Let M denote the total mass and $\mathbf{I}$ denote the inertia of the body. The dynamics of a rigid body are [7]

$$\dot{x} = v \tag{1}$$

$$M\dot{v} = RF \tag{2}$$

$$\dot{R} = R\Omega_\times, \tag{3}$$

$$\mathbf{I}\dot{\Omega} = -\Omega \times \mathbf{I}\Omega + \Gamma, \tag{4}$$

where $\Omega_\times$ denotes the skew-symmetric matrix such that $\Omega_\times v = \Omega \times v$. The exogenous force and torque inputs are denoted $F, \Gamma \in \{B\}$ respectively.

For a typical aerial robot capable of quasi-stationary flight a vectored thrust model is adequate for the purposes of control design and analysis [1], [6], [11], [19], [23]. The net force is modelled by

$$F := -Te_3 + MgR^\top e_3 + F_{\text{aero}} \tag{5}$$

where $T \in \mathbb{R}$ is a scalar input representing the thrust force applied in direction e_3, the unit vector with a one in the third entry, in this case representing the z-axis direction in the body-fixed-frame. The term F_{aero} denotes aerodynamic forces due to induced drag, gusts, so called small-body forces due to action of flaps for attitude control, etc, that are not explicitly modelled. Such forces are typically second order compared to the dominant thrust forces, at least in normal flight conditions.

B. Dynamics of the haptic device

The haptic user interface considered is one capable of motion in 3D-Euclidean space. A haptic device is typically a parallel manipulator, usually cable driven, with high performance torque controlled motors. The resulting dynamics are highly complex and depend on the configuration of the device. For a three degree of freedom haptic device the position of the joystick $\xi \in \mathbb{R}^3$ can be used as generalised coordinates for an Euler-Lagrange model of the system dynamics leading to a theoretical model of the system

$$m(\xi)\ddot{\xi} = C(\xi, \dot{\xi})\dot{\xi} - D(\xi)\dot{\xi} + G(\xi) + f + u \tag{6}$$

where $m(\xi)$ is the generalised mass matrix, $C(\xi, \dot{\xi})$ is a Coriolis matrix, $D(\xi) > 0$ is a damping matrix, $G(\xi)$ represents the force on the device due to gravity, f is the exogenous force applied to the joystick by the user, while u represents the force generated by the device actuators expressed with respect to the frame of reference attached to the joystick. In practice, the terms $m(\xi)$, $C(\xi, \dot{\xi})$, $D(\xi)$, and $G(\xi)$ are unknown for commercial systems. Instead, commercial haptic devices are provided with active control and a programming interface that, at least approximately, transforms the dynamics into those of a point mass moving in Euclidean space

$$m\ddot{\xi} = -D(\xi)\dot{\xi} + mge_3 + f + u, \tag{7}$$

with unknown damping term $D(\xi) > 0$. For high end haptic devices the damping term $D(\xi)$ can be ignored, however, for low cost devices, such as the device used in the experimental section, the damping can be quite significant.

C. Integrated system

We assume that the vehicle is equipped with an inertial measurement unit and suitable filter algorithm to produce robust high-bandwidth estimates of vehicle attitude R and angular velocity Ω. The most common (and simplest) approach to vehicle control is to design an inner-loop high-gain control for the system attitude, (3) and (4), [15]. The inner-loop regulates the torque inputs to track a desired orientation $R^*(t)$ while rejecting disturbances.

The haptic system is interfaced to the aerial robot by using the displacement of the haptic joystick from a central position to control translational force on the aerial robot

$$F_{\text{pilot}} := k_{\text{pilot}}\xi(t), \qquad k_{\text{pilot}} > 0$$

Define the desired translational force F^* to be the sum of two external forces F_{pilot} and F_{env}

$$F^*(t) = F_{\text{pilot}} + F_{\text{env}} \tag{8}$$

where F_{env} is the virtual force generated by the environment (see Section III).

Substituting for $F = F^*$, $R = R^*$ and $T = T^*$ into Eq. 5 and rearranging we obtain

$$MgR^{*^\top} e_3 - T^* e_3 = F^* - F_{\text{aero}} \tag{9}$$

where R^* and T^* are the desired attitude and thrust for the vehicle. Assuming that $F^* - F_{\text{aero}}$ remains bounded and fixing the desired yaw rotation around the axes e_3 as an exogenous input that will be separately specified by the pilot, then Eq. 9 can be uniquely solved for R^* and T^*. The desired orientation and thrust (R^*, T^*) are time-varying set-points for the inner high-gain control-loop implemented on the vehicle. We assume that the aerodynamic disturbances F_{aero} are second order compared to the dominant thrust control and are negligible in the attitude stabilised system. Thus, in this paper, we will consider only control of the translational dynamics, (1) and (2), with a direct control input $F \approx F^*$ provided by a suitable inner-loop high-gain controller.

The haptic system is far simpler to analyse. Define the internal force control (see Eq. 7) on the haptic system to be

$$u := mge_3 - C\xi + k_{\text{env}}F_{\text{env}} \tag{10}$$

for $k_{\text{env}} > 0$ a positive constant. The first term is used to cancel the gravitational effect on the joystick, the second

term creates a spring potential well around the centre point of the joystick, while the third term models the force feedback from the environment to the pilot.

The dynamics of the integrated system can be modelled by

$$\dot{x} = v \tag{11a}$$

$$M\dot{v} = R(k_{\text{pilot}}\xi(t) + F_{\text{env}}) + \Delta \tag{11b}$$

$$m\ddot{\xi} = -D(\xi)\dot{\xi} - C\xi + k_{\text{env}}F_{\text{env}} + f, \tag{11c}$$

where f is the force applied by the pilot to the haptic joystick, F_{env} is a virtual force that is generated by an optical impedance and $\Delta(t)$ is an unknown bounded load disturbance that is generated by the tracking error of F to F^* combined with the unknown aerodynamic disturbances F_{aero}.

The most important term in the model (11) is the environmental force F_{env}. For a vehicle that has no physical contact with its local environment, and hence has no direct velocity constraints, the environmental force is best modelled as an impedance. An impedance for the dual velocity/force variables of a rigid-body moving in free space is a, possibly time-varying, integro-differential mapping from velocity to force. In this paper, we will only consider static impedances, however, we will allow the impedance to depend non-linearly on the environment (and state) of the vehicles. Thus, we write

$$F_{\text{env}} := -\kappa_{\text{env}}(v) \in \mathbb{R}^3 \tag{12}$$

where $\kappa_{\text{env}}(v)$ is the impedance mapping.

If κ_{env} is a positive definite function of v, in the sense that $\langle v, \kappa_{\text{env}}(v)\rangle \geq 0$ then the impedance is termed *dissipative*[1]. That is, the dual variables velocity and force will dissipate the vehicle's kinetic energy and slow the vehicle down. Intuitively, the force F_{env} will always 'oppose' motion of the vehicle.

III. O I

Consider a continuous-time vision system. Assume that the environment in which the vision system moves is static and that the illumination is not varying with time. The optic flow is defined as the instantaneous observed velocity of image features in the image plane of the vision system. Mathematically it is a time-varying vector field $\Phi_t(p)$, where t is the time index and p is the pixel coordinates, defined on the image plane. Let $\Phi_{[t_1,t_2]}$ denote the optic flow for all time instances in the interval $[t_1, t_2]$.

Definition 3.1: Consider a continuous-time vision system with its focal point at the origin of the airframe and moving with the rigid-body dynamics given by (1)-(4). An *optical impedance* is a mapping

$$\kappa : (t, \Phi_{[-\infty,t]}) \mapsto \mathbb{R}^6$$

to the force and torque 'applied' by the vision system to the robot at time t

$$(F(t), \Gamma(t)) := \kappa\,(t, \Phi_{[-\infty,t]})$$

[1]The angle-brackets denote inner-product.

An optical impedance is termed *static* if κ only depends on the value of $\Phi_{[-\infty,t]}$ at time t; that is

$$(F(t), \Gamma(t)) := \kappa\,(t, \Phi_t)\,.$$

□

In this paper, we consider only the translational motion of the vehicle and the optical impedances considered will only act to produce environment forces F_{env} as per (11b) and (11c).

Definition 3.1 makes the dependence of optical impedance on the optical flow field of the vision system explicit, however, this is a very abstract construction and involves the whole vector field Φ as an input argument in the functional mapping. In practice, we propose an intermediary step where we define *optical motion cues*, finite dimensional features derived from the optic flow field $\Phi_{[-\infty,t]}$ (or Φ_t for a static impedance) that will simplify the process of defining the optical impedance. The approach is best illustrated by example.

Consider a spherical camera, that is one in which the image sequence is projected onto a sphere rather than the more usual flat image plane, moving freely in a 3D-environment. Denote coordinates on the spherical image surface by vectors $p \in S^2$, the sphere $S^2 = \{p \in \mathbb{R}^3 \mid |p| = 1\}$. Let $\lambda : S^2 \to \mathbb{R}$ denote a scalar field on the sphere with values denoting the distance from the focal point of the camera to the environment. We assume that the environment is rich in texture, that is that the optic flow is well defined at every point on the sphere and that the vision system is operating in continuous time. The optic flow Φ is a vector field $\Phi : S^2 \to TS^2$ on the sphere (where TS^2 denotes the tangent bundle of the sphere) given by [10]

$$\Phi(p) := -\Omega \times p - \frac{1}{\lambda(p)}\left(I_{3\times3} - pp^\top\right)V \tag{13}$$

where $I_{3\times3}$ is the 3×3 identity matrix, $V = Rv$ is the velocity represented in the body-fixed frame. Note the dependence of the optic flow on the inverse depth to the observed environment.

Consider the optical motion cue w_{mean} defined by the integral

$$w_{\text{mean}} = \int_{S^2} \Phi(p)dp \in \mathbb{R}^3 \tag{14}$$

where the vector $\Phi(p) \in T_pS^2 \subset \mathbb{R}^3$ is thought of as embedded in $\mathbb{R}^3$ and the resulting integration is just the vector comprising the integrals of the vector entries of $\Phi(p) \in \mathbb{R}^3$. The optical motion cue w_{mean} can be used to define an optical impedance κ_{mean} by

$$\kappa_{\text{mean}}(\Phi) := c_{\text{mean}}w_{\text{mean}} = c_{\text{mean}}\int_{S^2} \Phi(p)dp \in \mathbb{R}^3$$

where c_{mean} is a positive constant. The optical impedance κ_{mean} is a static dissipative impedance. To see that κ_{mean} is

dissipative we set $F_{\text{env}} = \kappa_{\text{mean}}(\Phi)$ and compute

$$\begin{aligned}\langle V, F_{\text{env}}\rangle =& V^\top \int_{s^2} \Phi(p) dp \\ =& -V^\top \int_{S^2} (\Omega \times p) dp - V^\top \int_{S^2} \frac{(I - pp^\top)}{\lambda(p)} V dp \\ =& -V^\top \int_{S^2_+} (\Omega \times p + \Omega \times (-p))\, dp \\ & - V^\top \left(\int_{S^2} \frac{(I - pp^\top)}{\lambda(p)} dp \right) V\end{aligned}$$

where the integral over the full sphere for the first term is rewritten over S^2_+, the upper hemisphere of the sphere with respect to an arbitrary choice of coordinates, and the lower hemisphere contribution is provided by the additional $-p$ term in the integrand. Define

$$Q_{\text{mean}} := \left(\int_{S^2} \frac{(I - pp^\top)}{\lambda(p)} dp \right) > 0.$$

and note that this is a strictly positive definite for a generic depth field λ. It follows that

$$\langle V, F_{\text{env}}\rangle = -V^\top Q_{\text{mean}} V \leq 0$$

and the impedance is shown to be dissipative.

Unfortunately, the optical impedance κ_{mean} does not lead to desirable characteristics of the teleoperation system. In particular, it has low sensitivity to a direct collision of the vehicle with an obstacle since the optic flow in the direction of motion is zero. Moreover, it is highly sensitive to optic flow orthogonal to the direction of motion, leading to high 'drag' force when manoeuvering along a wall but low resistance when actually moving towards the wall. In the next section we propose two optical impedances that lead to more desirable behaviour.

IV. O

In this section, a combination of two optical impedances are discussed that, we believe, taken together provide a good model for obstacle avoidance. The optical impedances chosen are similar in concept to the visual cues used by Coombs *et al.* [4].

A. Optical impedance for collision avoidance

The spherical divergence of the optical flow Φ is given by

$$\text{div}\Phi(p) = \frac{2p^\top V}{\lambda(p)} + \frac{\mathrm{d}\lambda(p) \cdot \Phi(p)}{\lambda(p)} \tag{15}$$

(see [5], [3]) The first term depends on the component of the velocity in the direction p and is scaled by the inverse distance to the environment. This is the primary information encoded in the divergence that provides a cue when the vehicle is moving towards or away from the obstacle. The second term depends on the expression $\mathrm{d}\lambda(p) \cdot V = \frac{d}{dt}\lambda(p)$ where p is a fixed direction on the sphere. The first term is highly desirable as an optical motion cue to avoid collisions. The second term, however, is primarily associated with the change in perspective of the environment and tends to be highly sensitive in directions orthogonal to the motion of the vehicle. Correspondingly, since the second term depends on the value of the optic flow Φ, it is zero when $p = V/|V|$ is taken in the direction of the velocity.

Define an optical motion cue

$$w_{\text{foe}} = \begin{cases} \text{div}\Phi(V/|V|) & \text{for } V \neq 0 \\ 0 & \text{for } V = 0 \end{cases}$$

where 'foe' stands for focus of expansion. In practice, it is possible to extract the translational optic flow from the full flow field by compensating the rotational component $\Omega \times p$ based on separate measurements of angular velocity. The direction of motion V will correspond to the focus of expansion of the translational flow that can easily be computed [14]. Since the divergence of full flow does not depend on the rotation, the optical motion cue w_{foe} is also the the divergence at the focus of expansion of the translational optic flow field.

Based on the optical motion cue w_{foe} we define an optical impedance

$$\kappa_{\text{foe}}(\Phi) := \begin{cases} -c_{\text{foe}} \frac{\text{div}\Phi\left(\frac{V}{|V|}\right)}{|V|} V & \text{for } V \neq 0 \\ 0 & \text{for } V = 0 \end{cases}$$

where $c_{\text{foe}} > 0$ is a constant. Note that $\kappa_{\text{foe}}(\Phi) \in \mathbb{R}^3$ as required and depends only on the value of $\Phi_t(p)$ at time t and is a static optical impedance.

A key mathematical property of the optical impedance $\kappa_{\text{foe}}(\Phi)$ is that it is *dissipative*. Defining $F_{\text{env}} = \kappa_{\text{foe}}(\Phi)$ and (for non-zero V) computing

$$\begin{aligned}\langle V, F_{\text{env}}\rangle =& -\frac{\text{div}\Phi\left(\frac{V}{|V|}\right)}{|V|} |V|^2 \\ =& -2\frac{|V|^2}{\lambda(V/|V|)}\end{aligned}$$

where the second line follows by substituting the value of $\text{div}\Phi$ from (15) for $p = V/|V|$ and noting $\Phi(V/|V|) = 0$.

The optical impedance $\kappa_{\text{foe}}(\Phi)$ is highly effective at preventing collisions with the environment surrounding the robot — creating a force feedback for the user that is intuitive and effective.

B. Corridor centring

The translational optic flow field obtained by compensating for the angular velocity is

$$\Phi_{\text{trans}} := \Phi + \Omega \times p$$

Assume that the direction of motion $V/|V|$ is computed from the focus of expansion of Φ_{trans} or some other method [14]. Define the equatorial circle

$$E_{\text{diff}} := \{p \in S^2 \mid \langle p, V\rangle = 0\}.$$

Note that E_{diff} is well defined as a circle for $V \neq 0$ while for $V = 0$ one has $E_{\text{diff}} = S^2$.

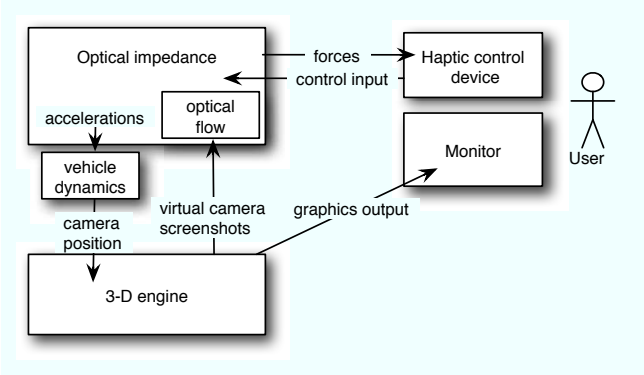

Fig. 1. Block diagram of the simulation environment.

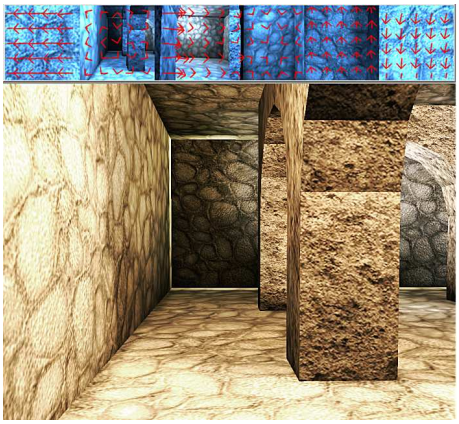

Fig. 2. Screenshot from the 3D simulation environment. The six small images on the top show the six cameras together with extracted optic flow, from left to right: left, front, right, back, up, down.

Define an optical motion cue by

$$w_{\text{diff}} := \begin{cases} \frac{1}{2}\int_{E_{\text{diff}}} \langle \Phi_{\text{trans}}(p_\theta), V\rangle \, p_\theta d\theta & \text{for } V \neq 0 \\ 0 & \text{for } V = 0 \end{cases}$$

where (for $V \neq 0$) the circle E_{diff} is parameterised by the angle θ and p_θ denotes the S^2 coordinates of the parameter. The optical motion cue w_{diff} compares the component of translational optic flow in the direction of motion at antipodal points orthogonal to the direction of motion. Since all vectors p_θ are orthogonal to V then w_{diff} is also orthogonal to V. Define the optical impedance to be

$$\kappa_{\text{diff}}(\Phi) := c_{\text{diff}} w_{\text{diff}}.$$

To understand the effect of the optical impedance $\kappa_{\text{diff}}(\Phi)$ imagine a vehicle moving down a corridor. The translational optical flow will be larger on the side of the vehicle that is closest to the wall of the corridor. This will generate a contribution to $\kappa_{\text{diff}}(\Phi)$ that will act to push the vehicle away from the closer wall towards the middle of the corridor.

A key mathematical property of the optical impedance $\kappa_{\text{diff}}(\Phi)$ is that it is *passive*. Defining $F_{\text{env}} = \kappa_{\text{diff}}(\Phi)$ one has

$$\begin{aligned} \langle V, F_{\text{env}}\rangle &= \frac{V^\top}{2}\int_{E_{\text{diff}}} \langle \Phi_{\text{trans}}(p_\theta), V\rangle \, p_\theta d\theta \\ &= \frac{1}{2}\int_{E_{\text{diff}}} \langle \Phi_{\text{trans}}(p_\theta), V\rangle \langle V, p_\theta\rangle d\theta \\ &= 0 \end{aligned}$$

since p_θ is orthogonal to the velocity V. As a consequence the differential flow optical impedance does not add or remove energy from the system. In practice, the operator will feel that the vehicle slides effortlessly along corridors and walls with the only forces applied helping steer the vehicle to the middle of the corridor.

C. Combined optical impedance

The optical impedance proposed as a practical choice combines the spherical divergence computed at the focus of expansion of the translational flow field along with the passive optical impedance calculated from differential flow of the translational flow field

$$\kappa_{\text{env}}(\Phi) := \kappa_{\text{foe}}(\Phi) + \kappa_{\text{diff}}(\Phi). \tag{16}$$

The resulting closed loop system has $F_{\text{env}} = \kappa_{\text{env}}(\Phi)$ and inherits the collision avoidance and corridor centring properties of its constituents.

V. I E R .

For this evaluation a virtual simulation environment was implemented (Figure 1). The simplified vehicle dynamics from (11) are used to simulate a force-actuated hovering vehicle. A measurement of optical flow is extracted from rendered real time images using OpenCV image processing algorithms. Optical impedance as described in section IV is computed and applied to the vehicle dynamics, and also to the 3-D haptic controller. The preliminary experiments are a precursor to trials with a 4-rotor flying platform, and serve as a proof of concept. Furthermore, the experiments provide insights into the stability of the theoretical system in the presence of un-modelled effects such as time lags, sparse optical flow and calibration errors in the spherical camera projection. The simulation and the haptic device can be seen in the accompanying video.

A. Simulation environment

The 3-D game engine *Irrlicht* was used to create an artificial indoor world. A screenshot of the simulation can be seen in Fig. 2. To obtain an approximation of spherical optical flow, six virtual perspective cameras with 100 x 100 pixels resolution are used (seen as thumbnails across the top of Fig. 2). We use the pyramidal implementation of Lucas-Kanade optical flow algorithm (OpenCV) to calculate a sparse optical flow vector field. Currently the spherical optical flow field is approximated by only six points on the sphere (given by the centre of each virtual camera). Divergence is calculated for each camera by convolution with a 3x3 gradient operator and summation. Although the image sequence is generated

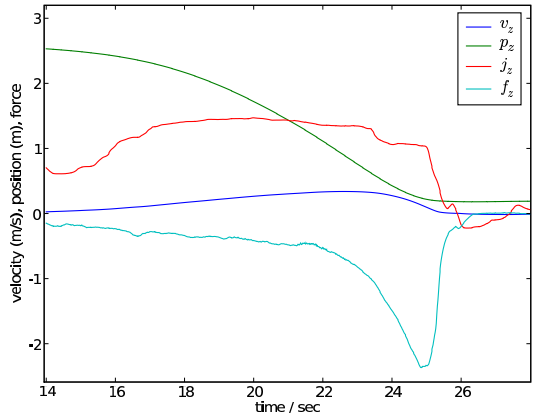

Fig. 3. Forward velocity v_z, distance to wall p_z, joystick input j_z and haptic force f_z while approaching a wall. The increase in repelling force caused by divergence div$\Phi(p)$ can clearly be seen.

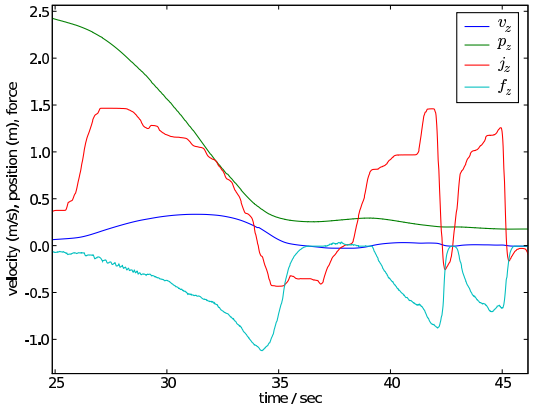

Fig. 4. Another approach towards a wall. The vehicle velocity drops to zero in close proximity to the wall, and the haptic device is pushed back against the operator's hand. The vehicle-internal feedback loop reduces the approach velocity despite multiple forward pushes of the joystick.

through a simulated environment there is still a significant amount of noise in the optic flow computation due to poor image texture, erroneous data correspondences, etc. We are confident that the results obtained indicate a robustness of the proposed approach to image noise.

To calculate the optical impedance forces on the vehicle according to (16) the direction of motion is required. In a real implementation this direction would be estimated from the optic flow using a technique such as proposed in [14], [16]. This cannot be reliably done using the six views available and we use the known velocity from the vehicle dynamics simulation. The optical impedance is then computed using (16), and by interpolating between the six cameras.

The computed haptic forces are sent to a 3-DOF haptic device (NovInt Falcon). A centring (spring) force and a small amount of damping is applied to the haptic device with an update rate of 1 kHz. The control software samples camera images from the 3-D engine at 40-50 frames per second for calculation of optical impedance. As two frames are required to compute flow, the total time lag of the vision system is approximately 50 ms. The setup can be seen in the included video submission.

B. Experimental results

The first experiment, Fig. 3, shows the behaviour of the system as the operator accelerates the vehicle towards a vertical wall. The haptic force f_z is proportional to the frontal divergence (with some moderate low pass filtering). It can be seen that the noise level of the divergence is sufficiently low to provide a clean force signal. Divergence measured from real image sequences in well-textured environments is comparable, provided the images have a good exposure and sufficient dynamic range. The sharp increase in force close to the wall is clearly visible in the plot, and can be perceived by the pilot. Due to the action of F_{env} the vehicle slows down even though the joystick is commanding full forward acceleration. As the operator gives in to the increasing force, the joystick moves backwards, and the vehicle stops. Letting

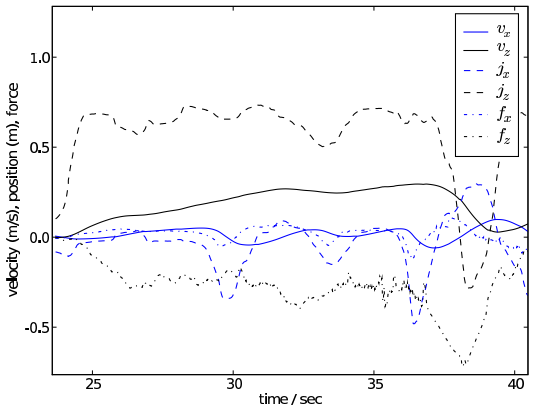

Fig. 5. Flying along a corridor with arches. The centring force f_x fluctuates caused by passing pillars on the right.

go of the control stick will always slow down the vehicle before it hits an obstacle, and can be regarded as a safe fall-back procedure. Theoretically the vehicle should also stop before impact even if the operator keeps accelerating forward. In practice divergence does not grow indefinitely — the rendered texture has limited resolution in the simulation, and in the real world the image will become blurred at close range as the camera has a fixed focal length (usually set at infinity). This is a practical limit to the amount of available dissipative virtual force. In practice, it was observed that an operator quickly learnt to read the force signals correctly and was able to fly close to the wall without colliding.

Fig. 4 shows a different test run, where the operator tries to push the vehicle into the wall. Despite a full scale joystick command, the velocity remains very low, and the distance to the wall only decreases very slowly. At the same time the haptic device applies large opposite forces against the attempted action. This simulation shows an initial approach and then two additional attempts to approach the wall.

Finally, Fig. 5 shows the centring forces while the vehicle is flying along a corridor between the wall on the left hand side and arches and pillars on the right (see Fig. 2). As the

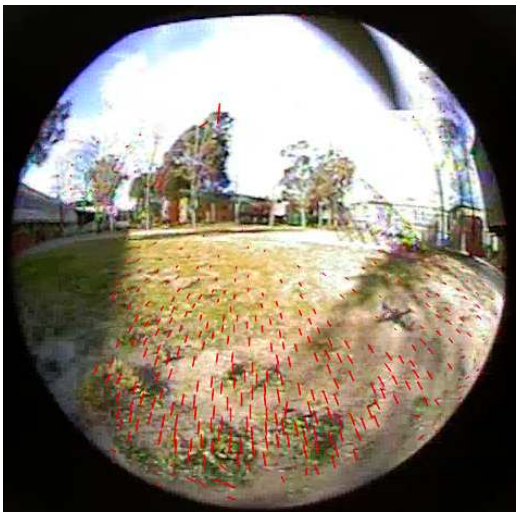

Fig. 6. Optic flow extracted from on-board video camera of the *Hummingbird* quad-rotor aerial robot.

vehicle passes a pillar, a centring force is applied to the haptic device. The induced lateral motion of the control stick steers the vehicle clear of the obstruction towards the center of the corridor.

VI. CONCLUSIONS AND FUTURE WORK

We proposed the concept of *optical impedance* to provide haptic feedback and vehicle stabilisation in a teleoperation context. The forces applied to the vehicle (by the vision system's control input to the propulsion of the vehicle) are dissipative (frontal divergence) or passive (centring force), and therefore stabilise the vehicle relative to its environment, which is a safe fallback position if there is no active operator input. The operator receives clear haptic repelling force feedback prior to collisions with objects, and additional centring forces when flying through narrow passageways. Future research will investigate additional intuitive haptic cues, and application-specific haptic guidance.

The described method is now being implemented on a 4-rotor hovering vehicle, using "fish-eye" wide angle cameras which provide a better approximation to a spherical camera. An example frame from the vehicle's video stream, with overlaid optical flow, is shown in Fig. 6. The interested reader can also find initial experimental results implemented on a holonomic ground vehicle in [22].

R

[1] R. Bradley. The flying brick exposed: nonlinear control of a basic helicopter model. Technical Report TR/MAT/RB/6, Department of Mathematics, Glasgow Caledonian University, Scotland, U.K., 1996.

[2] J. S. Chahl, M. V. Srinivasan, and S. W. Zhang. Landing strategies in honeybees and applications to uninhabited airborne vehicles. *The International Journal of Robotics Research*, 23:101–110, Feb 2004.

[3] R. Cipolla and A. Blake. Surface orientation and teim to contact from image divergence and deformations. In *Proceedings European conference on computer visiion*, pages 187–202, 1992.

[4] D. Coombs, M. Herman, T. Hong, and M. Nashman. Real-time obstacle avoidance using central flow divergence and peripheral flow. *IEEE Transactions on Robotics and Automation*, 14(1):49–59, 1998.

[5] Z. Duric, A. Rosenfeld, and J. Duncan. The applicability of greens theorem to computation o f rate of approach. *Internationa journal of computer vision*, 31(1):83–98, 1999.

[6] M. Dahlen E. Frazzoli and E. Feron. Trajectory tracking control design for autonomous helicopters using a backstepping algorithm. *Proceedings of the American Control Conference ACC*, pages 4102–4107, 2000.

[7] H. Goldstein. *Classical Mechanics*. Addison-Wesley Series in Physics. Addison-Wesley, U.S.A., second edition, 1980.

[8] W.E. Green, P.Y. Oh, and G. Barrows. Flying insect inspired vision for autonomous aerial robot maneuvers in near-earth environments. In *IEEE International Conference on Robotics and Automation*, volume 3, pages 2347–2352, April 2004.

[9] Nicolas Guenard, Tarek Hamel, Vincent Moreau, and Robert Mahony. Design of a controller allowed the intuitive control of an x4-flyer. In *Proceedings of the 8th International IFAC Symposium on Robot Control, SYROCO 2006*, pages –, Bologna, Italy, September 2006. International Federation of Automatic Control.

[10] T. Hamel and R. Mahony. Visual servoing of an under-actuated dynamic rigid-body system: An image based approach. *IEEE Transactions on Robotics and Automation*, 18(2):187–198, April 2002.

[11] T. Hamel, R. Mahony, R. Lozano, and J. Ostrowski. Dynamic modelling and configuration stabilization for an X4-flyer. In *Proceedings of the International Federation of Automatic Control Symposium, IFAC 2002*, Barcelona, Spain, 2002.

[12] M. Ichikawa, H. Yamada, and J. Takeuchi. Flying robot with biologically inspired vision. *Journal of Robotics and Mechatronics*, 13(6):621–624, 2001.

[13] D.N. Lee. A theorey of visual control of braking based on information about time to collision. *Perception*, 5(4):437–459, 1976.

[14] John Lim and Nick Barnes. Directions of egomotion from antipodal points.

[15] R. Mahony, P. Corke, and T. Hamel. Dynamic image-based visual servo control using centroid and optic flow features. *Journal of Dynamical Systems, Measurement and Control*, 130(1):011005 (12 pages), January 2008.

[16] C. McCarthy and N. Barnes. Performance of optical flow techniques for indoor navigation with a mobile robot. In *Proceedings of the IEEE International Conference on Robotics and Automation*, pages 5093–5098, 2004.

[17] R.C. Nelson and J.Y. Aloimonos. Obstacle avoidance using flow field divergence. *IEEE Transactions on Pattern Analysis and Machine Intelligence*, 11(10):1102–1106, 1989.

[18] T. Netter and N. Franceschini. A robotic aircraft that follows terrain using a neuromorphic eye. In *Proceedings of the 1997 IEEE/RSJ International Conference on Intelligent Robots and Systems, IROS '97*, volume 2, pages 129–134, Sept. 1997.

[19] P. Pounds, R. Mahony, P. Hynes, and J. Roberts. Design of a four-rotor aerial robot. In *Australasian Conference on Robotics and Automation Conference, ACRA-2002*, Auckland, New Zealand, 2002.

[20] F. Ruffier and N. Franceschini. Visually guided micro-aerial vehicle: Automatic take off, terrain following, landing and wind reaction. In *Proceedings of the IEEE International Conference on Robotics and Automation*, pages 2339–2346, New Orleans, LA, April 2004.

[21] F. Ruffier and N. Franceschini. Optic flow regulation: The key to aircraft automatic guidance. *Robotics and Autonomous Systems*, 50:177–194, 2005.

[22] Felix Schill, Robert Mahony, Peter Corke, and Luke Cole. Virtual force feedback teleoperation of the insectbot using optic flow. In *Proceedings of the Australasian Conference on Rotoics and Automation*, Canberra, Australia, December 2008.

[23] O. Shakernia, Y. Ma, T. Koo, and S. Sastry. Landing an unmanned air vehicle: Vision based motion estimation and nonlinear control. *Asian Journal of Control*, 1(3):128–145, 1999.

[24] M.V. Srinivasan and S. Zhang. Visual motor computations in insects. *Annual Review of Neuroscience*, 27:679–696, July 2004.

[25] M.V. Srinivasan, S.W. Zhang, J.S. Chahl, E. Barth, and S. Venkatesh. How honeybees make grazing landings on flat surfaces. *Biological Cybernetics*, 83(3):171–183, August 2000.

[26] R. Zbikowski. Fly like a fly. *IEEE Spectrum*, 42(11):46–51, Nov. 2005.